IEEE Access
Multidisciplinary | Rapid Review | Open Access Journal

IEEE POWER & ENERGY SOCIETY SECTION

Received 11 January 2022, accepted 27 January 2022, date of publication 7 February 2022, date of current version 11 July 2022.

Digital Object Identifier 10.1109/ACCESS.2022.3149918

Development of a Low-Speed High-Efficiency PMSM and Its Drive System for Electric Windlass and Mooring Winch

GUI-HOU ZHOU[1,2], MING-ZHONG QIAO[1], XIAO-FENG ZHANG[1], JIN-HUI XIE[2], QING-LIANG HAO[2], CONG WAN[2], AND YONG ZHOU[2]

[1]College of Electrical Engineering, Naval University of Engineering, Wuhan 430033, China
[2]Wuhan Institute of Marine Electric Propulsion, Wuhan 430064, China

Corresponding author: Ming-Zhong Qiao (qiaomingzhong@126.com)

This work was supported by the MIIT High-Tech Ship Deck Machinery Quality Brand Special Project "Development of Permanent Magnet High-Efficiency Motor" under Grant MC-2016-P04-05.

ABSTRACT Permanent magnetization of electric windlass and mooring winch (EWMW) has become a research trend in the development of new generation deck machinery. The paper investigates the development of a low-speed and high-efficiency permanent magnet synchronous motor (PMSM) and its drive system based on the load characteristics and special requirements of an EWMW. Firstly, the design specifications and key points of the motor drive system are analyzed. Secondly, a design method of parameter matching is proposed to design a 110 kW 75 r/min PMSM based on finite element method, field circuit coupling, and co-simulation. Finally, a prototype is developed and applied to a 45 T EWMW. The test results show that the PMSM can attain an efficiency of 94.3% at the rated operation, good traction characteristics with high torque at low speed, and 3 times wide flux-weakening region at constant power. Therefore, the matching design method is effective in the design of PMSM and drive system for EWMW.

INDEX TERMS Permanent magnet synchronous motor (PMSM), electric windlass and mooring winch (EWMW), design, drive system.

I. INTRODUCTION

Windlass is an important navigation device for ships. Windlass and mooring winches (WMW) are combined into one device at the bow to realize the dual use of one machine in most ships. Its operation performance directly affects the safety of ships. When any one of them has a fault, the ship is not allowed to sail. Therefore, they are vital to ships [1]–[3].

The load of the WMW is large. A multi-working condition under variable load requires that the drive system can start quickly and stop accurately. The traditional hydraulic-driven WMW has many problems, such as low efficiency, slow system response, complicated pipeline pavement (requiring independent pressure supply system), large space occupation, hydraulic oil leakage, and complex intelligent control, whereas EWMW has many advantages in terms of reliable operation, fast response, easy maintenance, no risk of oil pollution, and high efficiency. Therefore,EWMW has been widely used in ships. However, most EWMWs are driven by pole changing motor, winding motor based on the silicon-controlled rectifier, and asynchronous variable frequency motor [4]. Moreover, the high reliability, low noise and vibration, high efficiency, energy-saving, and intelligent integration of EWMWs are required with the development of the deck machinery. Therefore, low-speed, high torque, wide-speed regulation, and high-efficiency PMSMs have become the trend and research hotspot of the new generation of deck machinery.

Due to the advantages of high-power density, high power factor, and high efficiency, PMSMs have gained a long-term development in automotive traction, wind power generation, ship electric propulsion, electric vehicle, and rail transportation [5]–[8]. Most reported studies have focused on the analysis and optimization of the electrical parameters, thermal analysis of motor, vibration,and noise, and influence of the PM materials [9]–[15]. For low-speed PMSM, it is mainly used in wind power generation, ship electric propulsion, and coal mine direct drive system [16]–[18].

The associate editor coordinating the review of this manuscript and approving it for publication was Valentine Novosad.

Literature [19] investigated the design criteria for a high-efficiency PMSM. This method does not seek to simply reduce the electromagnetic load, but to optimize a set of motor design variables without increasing the overall size, which is usually imposed as a design constraint. Generally speaking, low speed and high efficiency are contradictory to permanent magnet motors. A lot of research on constant power demagnetization speed regulation has been applied to electric vehicles. Literature [20]–[22] focused on how to improve the speed range and power density, whereas there are few studies on the design of PMSM in deck machinery EWMW considering special load characteristics.

In this paper, according to the load characteristics and special requirements of the EWMW, the design difficulties and key points of the low-speed and high-efficiency permanent magnet motor and drive system are presented. A method of parameter matching is proposed to design a low-speed and high-efficiency permanent magnet motor based on finite element method, field circuit coupling, and co-simulation. The correctness and effectiveness of the matching design method are verified through the experimental study of a 45 T EWMW.

II. DESIGN DIFFICULTIES AND KEY POINTS OF PMSM AND DRIVE SYSTEM OF EWMW

The duty type of the EWMW is S2, which has the characteristics of variable working conditions and multiple load spectrum. And the work conditions are divided into dynamic anchoring, free anchoring, anchor chain retraction, earth breaking, anchor bolt retraction, anchor bolt retraction to the outlet, and anchor bolt retraction to anchor lip. The work style of the winch is divided into the mooring, cable releasing, and drum constant tension. At the same time, the new generation of deck machinery is developing towards the direction of green, energy-saving, environmental protection, intelligence, stronger operation ability, and more complex structure and functional configuration. The power drive system requires a compact structure, high efficiency, strong overload capacity, good low-frequency characteristics, zero speed hover, constant tension control, fast response. Therefore, the design of the PMSM and drive system becomes more difficult.

A. DESIGN KEY POINTS OF PMSM

1) LOW-SPEED AND HIGH-EFFICIENCY

The PMSM with low-speed and high-efficiency is designed to eliminate the multi-stage gear and improve the transmission efficiency of the drive system, which needs to reasonably allocate the loss, optimize the ratio between the effective length and the inner diameter of iron-core, and overcome the assembly process of the winding under the conditions of ultra-deep slot multi-winding and limited end length.At the same time, improving the machining and assembly accuracy of motor components is also an important way to improve the efficiency.

2) WIDE FLUX-WEAKENING REGION SPEEDADJUSTABILITY

The PMSM needs to have three times the speed adjusts the capacity of flux-weakening to respond quickly and improve the efficiency of retracting and unwinding anchor chains and cables. And this poses a challenge to the rotor magnetic circuit topology design of the PMSM and the control of the frequency converter.

3) HIGH IMPACT RESISTANCE

The PMSM of the EWMW needs to bear a high impact load due to the influence of the structure itself, sea conditions, and geology. Therefore, special requirements are put forward for the design of the bearing, the length of the air gap, the structural strength, and the type of selection of the rotor position signal.

4) HIGH TORQUE ELECTROMAGNETIC BRAKE WITH SHAFT

The EWMW needs to have the function of quick automatic braking and emergency braking. Therefore, the PMSM should have an electromagnetic brake with high torque. According to the specification, the general working model of electromagnetic braking is to turn on the power to release the brake and turn off the power to the brake. Thus, the special design of the electromagnetic brake and the reduction of the interference to the position detection signal is put forward as new requirements because the position accuracy error will lead to low-speed jitter and low-speed creep.

When the motor runs at high speed in the field weakening area, if it is cut off or stopped under fault, the terminal voltage of the motor will rise suddenly due to the existence of back EMF. At this time, the braking of the brake will also help to protect the power devices of variable frequency drive.

B. DESIGN FEATURE OF VARIABLE FREQUENCY DRIVE SYSTEM

1) CONSTANT TENSION CONTROL ALGORITHM

Different from the torque control mode of the conventional PMSM, EWMW constant tension control needs to add a tension control ring outside the torque ring. The variable frequency driver receives the feedback analog signal of the tension sensor and the tension-given signal for closed-loop control. The PI parameters of the closed-loop control need to be set in combination with the parameters and the actual load of PMSM.

2) THERMAL DESIGN OF INVERTER UNDER EXTREME WORKING CONDITIONS

The thermal design of the frequency converter should be significant because the EWMW requires extreme working conditions such as 2.3 times of high overload capacity and zero speed hovering full torque, which involves the selection of IGBT and switching frequency.

3) ELIMINATION AND SUPPRESSION OF LOW-FREQUENCY TORQUE RIPPLE

The elimination of torque ripple is generally carried out from the design and control of the PMSM. Among them, the ripple torque is mainly suppressed by improving power supply high order harmonics and injecting harmonic method.

III. A METHOD OF PARAMETER MATCHING DESIGN OF PMSM

It can be seen from the above analysis that the design of low-speed and high-efficiency permanent magnet motor for EWMW has its particularities and difficulties, which not only involves the motor itself but also is closely related to the control strategy of the driving system. Thus, the selection of parameters cannot be designed by conventional methods, and matching design must be combined with control synthesis. In this paper, a co-simulation of the method based on finite element and field-circuit coupling is presented. The specific method flow chart is shown in Fig. 1. From Fig.1, the key idea is the parameters with a high weight ratio match the special requirement of EWMW, and the initial scheme is completed by using the finite element method and field-circuit coupling, and when combined with the control requirement of EWMW. Motor Solve and Simulink are used to carry out the co-simulation, the second iteration is completed, and the motor parameter design and control parameters are finally determined. In addition, the adaptive and matching design for EWMW is also mainly related to the high weight ratio parameters and electromagnetic brake and signal anti-interference design, cooling, oil-proof seal, and protection class in the structural design.

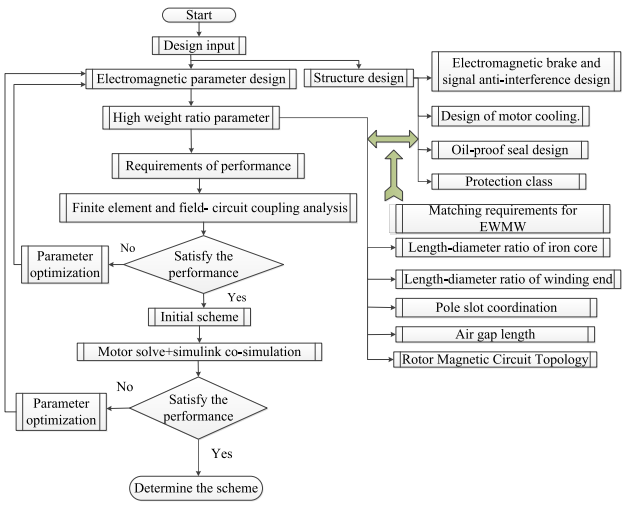

FIGURE 1. Flowchart of motor matching design method.

A. PARAMETER AND ADAPTIVE DESIGN OF PMSM

1) COPPER LOSS OF STATOR

The iron loss of the low-speed and high-efficiency PMSM is very small because of the low operating frequency, lower yoke magnetic density, and the low loss of thin silicon steel sheet, whereas the stator copper loss is very large. Therefore, the key point of parameter design is to reduce stator copper consumption on the premise of ensuring the overall dimension of the stator. The optimization direction is derived according to the following estimation formula of stator copper consumption.

The copper loss of stator can be approximated as

$$p_{cu} \propto J^2 m_{cu} \tag{1}$$
$$m_{cu} \propto \Delta_{\mathrm{cu}} D_{i1}^2 (K_L + K_1) \tag{2}$$
$$\Delta_{cu} \propto A/J \tag{3}$$
$$K_{\mathrm{L}} = la/D_{i1} \tag{4}$$
$$K_1 = \tau_{\mathrm{y}}/D_{i1} cos\alpha = \pi(1 + h_s/D_{i1})\beta/2pcos\alpha \tag{5}$$

where J is the current density of stator armature winding, $m_{cu}$is the weight of stator cooper, Δ_{cu} is the equivalent thickness of the armature surface conductor, D_{i1} is the inner diameter of stator, A is specific electric loading, K_L is length-inner diameter ratio of the iron core, $K_1$is the winding end- inner diameter ratio of the iron core, τ_{y} is the winding pole pitch, h_s is equivalent slot height, $\beta$is the winding short distance coefficient, $\cos\alpha$ is the cosine of the Angle between the end of the winding and the horizontal line, and $p$is the number of pole pairs of the rotor.

Substituting (2)-(5) to (1), the copper loss of stator is

$$p_{\mathrm{cu}} \propto AJD_{i1}^2 (K_L + K_1) \tag{6}$$

It is well known that the $D_{i1}^2 l_{\mathrm{a}}$ is the constant value when the torque of the motor is fixed. Therefore, (6) can be rewritten as

$$p_{\mathrm{cu}} \propto AJ(K_L^{1/3} + K_1 K_L^{-2/3}) \tag{7}$$

From (7), the copper loss of stator takes the minimum value when the K_L is equal to $2K_1$.

Then, the minimum of the copper loss is

$$min(p_{cu}) \propto AJK_1^{1/2} \tag{8}$$

Based on the above equations, the major conclusions are listed as follows:

(1) The copper loss of the stator is directly proportional to the thermal load. The copper loss of the motor can be reduced with the decrease of the thermal load.
(2) The copper loss of the stator can be reduced by selecting the aspect ratio K_L that is equal to $2K_1$ or approximately equal.
(3) By choosing a larger pole pair p value, the end length can be reduced, then to reduce the copper loss of the motor.
(4) The copper loss of stator can be reduced by controlling the ratio of groove height to inner diameter or increasing the full rate of groove.

It can be shown that the length-inner diameter ratio of iron core and winding end, pole pairs, slot size, and heat load are the high weight ratio parameters affecting the design

of low-speed and high-efficiency PMSM, which provides an optimization direction for the scheme matching design. At the same time, it can also be seen that the design difficulty and process realization of low-speed and high-efficiency PMSM, especially under the condition of the limited overall size of the new generation of EWMW.

2) AIR GAP LENGTH AND POLE SLOT COORDINATION

To meet the requirements of anti-shock design, the motor air gap is designed to be a larger value under the premise of meeting the performance, which is chosen to be 3 mm in this paper.

As mentioned above, the copper loss decreases as the number of pole pairs increases, thereby increasing the efficiency of the PMSM. In addition, the increase in the number of slots makes the stator slots tend to be long and narrow, which makes it difficult to embed and leads to an increase in slot leakage resistance. The number of stator slots is determined by the number of slots per phase for each pole q. Considering vibration and noise, q is generally an integer of 2-4. In this study, p is 12 and q is 2.

3) ROTOR MAGNETIC CIRCUIT TOPOLOGY

The rotor is usually equipped with an interior-type radial rotor topology to improve the wide-speed regulation and weak magnetic region. The general approach is to improve the weak magnetic effect by reducing the Quadrature-axis inductance *Lq*, increasing the Direct-axis synchronous inductance *Ld,* increasing the limit voltage and limit current of the motor, reducing the permanent magnet flux, and other measures. The distance between adjacent magnetic poles, the implantation depth of the magnetic pole center [23], and the design of the rated voltage point are the high weight ratio parameters that affect the effect of the weak magnetic field.

Literature [24] proposed and analyzed a kind of internal segmental rotor magnetic circuit structure that could effectively increase the direct-axis inductance, and the direct-axis inductance increased significantly, and the weak magnetic energy was improved. Considering the 3 times of weak magnetic field, the rotor topology adopted in this paper is interior PM type ''V'' and ''Segmented - shape''

4) ADAPTIVE DESIGN

The adaptive design of the EWMW mainly includes the protection class of IP56, the oil-proof seal design at the transmission end, the large-torque electromagnetic brake and the torque transmission design of the shaft, the design of preventing the interference of the electric field of the brake on the position sensing signal, and the cooling design of the motor.

B. MAIN PARAMETERS AND STRUCTURE OF PMSM

The main parameters of 110 kW and 75 r/min PMSM for a 45 T EWMW are listed in TABLE 1. The structure diagram of the PMSM is shown in Fig.2. The rotor adopts interior PM type ''V'' and ''Segmented - shape''; The electromagnetic brake adopts the structure of polygon friction pair in the rectified high strength friction disc. Position signal monitoring using a large gap of the reluctance type rotary transformer and the installation of the transition plate using non-magnetic materials to reduce the brake on the signal interference; The motor adopts a natural cooling design.

TABLE 1. Main parameters of the PMSM.

Parameter	Symbol	Value
Rated power/kW	P	110
Rated torque/ kN.m	T_N	14
Rated speed/rpm	n_N	75
Maximum speed /rpm	Nax	225
Rated line voltage/V	U	285
Phase	m	3
Number of Poles	$2p$	24
Number of stator slots	Z	144
Stator inner diameter/mm	$Di1$	930
Stator outer diameter/mm	$D1$	1150
Core axial length/mm	la	285
Stator skewed slot pitch	Sk	1
Air gap length / mm	g	3
Wire diameter	ϕd	90- Φ 1.12
Number of Conductors	Ns	6
length-inner diameter ratio	K_L	0.3064
winding end-diameter ratio	K_1	0.15

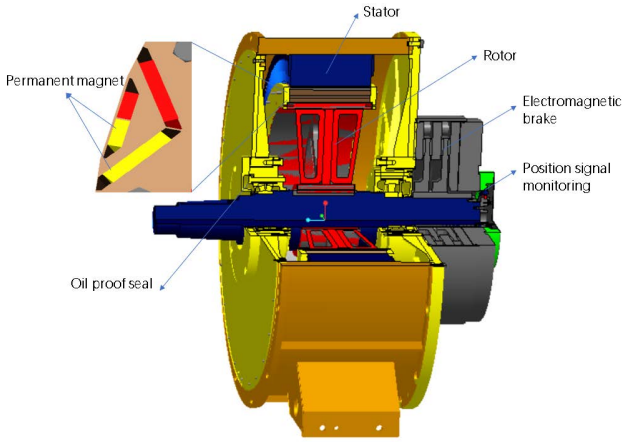

FIGURE 2. Schematic view of the PMSM(stator windings are not shown).

C. DESIGN OF DRIVE FREQUENCY CONVERTER

1) MASTER TOPOLOGY SCHEME

The main loop topology of the inverter adopts a modular ACDC-AC topology scheme. The rectifier part of the converter adopts mature and reliable 6-pulse rectifier technology to reduce the loss of the converter. And the rectifier inlet line is equipped with a 2% input line reactor to reduce the influence of the uncontrolled rectifier device on the grid side. The output side of the frequency converter with a dv/dt filter is provided to reduce the output dv/dt of the frequency converter. The single-line diagram of the main circuit and the schematic diagram of the inverter component are shown

in Fig. 3 and Fig. 4, respectively. The central unit controlling the inverter is adopted DSP28335+cpld(Complex programming logic device), and the dead time of transistors is about 2.1us. IGBT switching frequency is set to 2kHz.The signal of the rotary transformer is input into DSP28335 through the position sampling board, and the motor speed is calculated in real-time through the speed sampling function to achieve the closed-loop speed regulation function. The signal collected by the current sensor is input to DSP28335 through the current sampling sample, and the current is calculated in real- time.

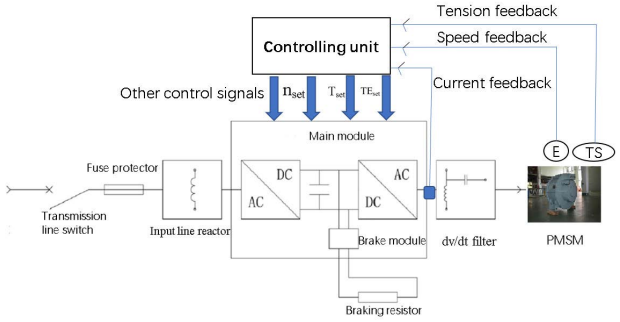

FIGURE 3. Single line diagram of the main circuit.

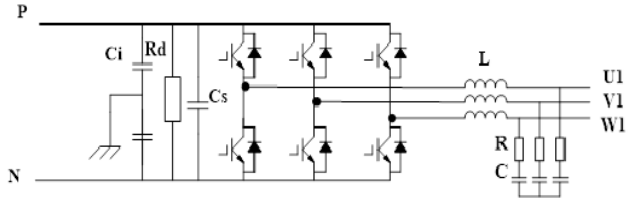

FIGURE 4. Inverter component schematic diagram.

2) CONTROL FLOWCHART

The EWMW winch can adjust the retracting and unwinding of the winch according to the tension of the cable. Therefore, the tension can be stabilized at an ideal value. The control process includes speed control, torque control, and constant tension control, as shown in Figure 5.

3) LOSS CALCULATION AND THERMAL ANALYSIS

The EWMW withstands extreme working conditions and the special requirement of 98% efficiency. And the loss calculation and thermal design calculation are carried out. The loss and temperature of frequency converter calculated by the thermal simulation analysis software are listed in TABLE 2.

As listed in TABLE 2, the efficiency is greater than 98%, and the temperature rise of the device meets the requirements.

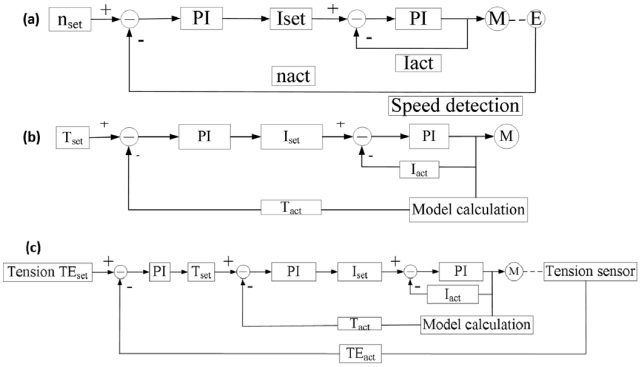

FIGURE 5. Control flowchart in a, b, and c, the alphabet subscripts set, and act represent the given value and the actual measured value, respectively. e.g., n_{set} and nact indicate the given speed value and the actual measured speed value, respectively.

TABLE 2. Loss and temperature of inverter.

Item	Parameter	Value
Loss	Diode loss in rectifier unit /W	389.9
	IGBT loss of inverter unit / W	1170.6
	Loss of input line reactor/ W	150.0
	Loss of outgoing reactor / W	180.0
	Another losses/ W	100.0
	Total loss/ W	1990.5
	Rated input power of frequency converter / W	119600
	Frequency converter efficiency /%	98.3
Temperature （environment temperature 50°C）	IGBT/ °C （Rated load）	94.4
	IGBT/ °C （2.3times rated load）	119.2
	Rectifier diode / °C （2.3times rated load）	101.7
	Braking resistor / °C	89.4

IV. DESIGN AND JOINT SIMULATION ANALYSIS BASED ON FINITE ELEMENT

A. BASIC MODEL OF ELECTROMAGNETIC FIELD CALCULATION

The transient electromagnetic field calculation model of the PMSM can be described as follows:

$$\begin{cases} \Omega 1 : \nabla \times (v\nabla \times A) == -J_s \\ S1 : A_Z = 0 \\ L : V_1 \dfrac{\partial A}{\partial n} = V_2 \dfrac{\partial A}{\partial n} - J_m \end{cases} \tag{9}$$

where Ω1 is the calculation region, $S1$ is Dirichlet boundary condition, v is the reluctivity, J_s and J_m are armature winding current density and permanent magnet boundary equivalent surface current density,respectively, A_Z is magnetic vector potential, n is normal unit vector outside the boundary of a permanent magnet, V_1 and V_2 are Non-permanent magnet region and permanent magnet region, respectively.

The three stator phase windings which are Y-connected with neutral are shown in Fig.6. Their induced voltages are given as e_a, e_b, and e_c, respectively, u_a, u_b, and u_c are the phase voltage, $u_n$is the potential of the neutral n, and their currents are given as i_a, i_b, and i_c, respectively, where subscripts a, b and c represent the three stator phase windings. R_1 and

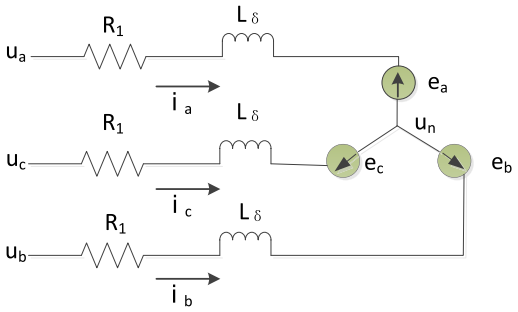

FIGURE 6. Stator circuit model of PMSM.

L_δ are the resistance and end-winding leakage inductance of the stator winding per phase, respectively.

From Fig. 6, the voltage and current equations are as follows [25]:

$$\begin{cases} \mathrm{e}_a + R_1 \mathrm{i}_a + L_\sigma \dfrac{\partial \mathrm{i}_a}{\partial t} = \mathrm{u}_a - \mathrm{u}_n \\ \mathrm{e}_b + R_1 \mathrm{i}_b + L_\sigma \dfrac{\partial \mathrm{i}_b}{\partial t} = \mathrm{u}_b - \mathrm{u}_n \\ \mathrm{e}_c + R_1 \mathrm{i}_c + L_\sigma \dfrac{\partial \mathrm{i}_c}{\partial t} = \mathrm{u}_c - \mathrm{u}_n \end{cases} \tag{10}$$

Three-phase windings are connected in a star shape, then the three-phase current satisfies the constraint that the sum of current is 0:

$$\mathrm{i}_\mathrm{a} + \mathrm{i}_\mathrm{b} + \mathrm{i}_\mathrm{c} = 0 \tag{11}$$

For operation from a balanced three-phase system,

$$\mathrm{u}_a + \mathrm{u}_b + \mathrm{u}_c = 0 \tag{12}$$

u_n is obtained by adding each side of (9) and then applying (10) and (11)

$$\mathrm{u}_\mathrm{n} = -\frac{\mathrm{e}_\mathrm{a} + \mathrm{e}_\mathrm{b} + \mathrm{e}_\mathrm{c}}{3} \tag{13}$$

Substituting (13) into (10), the voltage and current equations are given by

$$\begin{cases} \dfrac{1}{3}(2\mathrm{e}_a - \mathrm{e}_b - \mathrm{e}_c) + R_1 \mathrm{i}_a + L_\sigma \dfrac{\partial \mathrm{i}_a}{\partial t} = \mathrm{u}_a \\ \dfrac{1}{3}(-\mathrm{e}_a + 2\mathrm{e}_b - \mathrm{e}_c) + R_1 \mathrm{i}_b + L_\sigma \dfrac{\partial \mathrm{i}_b}{\partial t} = \mathrm{u}_b \\ \dfrac{1}{3}(-\mathrm{e}_a - \mathrm{e}_b + 2\mathrm{e}_c) + R_1 \mathrm{i}_c + L_\sigma \dfrac{\partial \mathrm{i}_c}{\partial t} = \mathrm{u}_c \end{cases} \tag{14}$$

The electromotive force of the stator winding is the key parameter that combines the field and circuit in the stator region.

In the stator windings region, the field calculation model is as follows

$$\frac{\partial}{\partial \mathrm{x}}(v\frac{\partial A}{\partial \mathrm{x}}) + \frac{\partial}{\partial \mathrm{y}}(v\frac{\partial A}{\partial \mathrm{y}}) = -\mathrm{J}_\mathrm{s} \tag{15}$$

The stator current is unknown, and the stator electric density J can be expressed as follows

$$J_\mathrm{s} = \frac{N_1}{aS_\mathrm{b}}(\alpha_\mathrm{a}\mathrm{i}_\mathrm{a} + \alpha_\mathrm{b}\mathrm{i}_\mathrm{b} + \alpha_\mathrm{c}\mathrm{i}_\mathrm{c}) \tag{16}$$

where N_1 is turn of a coil, a is a number of parallel branches, S_b is the area occupied by one coil edge, α_a, α_b and α_c is Winding current coefficient of the unit, respectively. e.g., when the unit belongs to A-phase winding, the positive phase band α_a value is 1, the negative phase band α_a value is -1, and the value in other cases is 0.

Take the A-phase winding for example, the electromotive force of the stator winding can be given as follows [26]

$$\mathrm{e}_\mathrm{a} = -\frac{\mathrm{d}\psi_\mathrm{a}}{\mathrm{dt}} = -\frac{\mathrm{d}}{dt}\left(\frac{N_1 pla}{as_b}\sum \alpha_a \Delta_e \frac{A_i + A_j + A_m}{3}\right) \tag{17}$$

In A_i, A_j and A_m are three different nodal magnetic potentials in the triangle. Δ_e is the area of the unit, so the same goes for B-phase winding and C-phase winding.

$$\mathrm{T}_\mathrm{cm} - \mathrm{T}_\mathrm{L} = \mathrm{J}\frac{\mathrm{d}\Omega}{dt} \tag{18}$$

Here T_em is the electromagnetic torque, T_L is the load torque, and Ω is the angular velocity, J is the moment of inertia.

Therefore, we can obtain the vector potential and currents at the same time by solving Eq. (9) and Eqs. (14), (16), (17), and (18) simultaneously. The above equations are discretized by the weighted residual method, and the coupled equations can be solved by the time-step Newton Raphson iterative method.

One simulation model based on field-circuit coupling analysis is shown in Fig.7.In this study, the equivalent resistance of the phase winding is 0.0351 Ω, and the leakage inductance of the phase end is 0.205 mH.

B. ELECTROMAGNETIC FIELD CALCULATION AND ANALYSIS

The FFT of no-load back EMF with the skewed slots, the torque curve under rated load and 3 times weak magnetic field, the FFT of current and terminal voltage under 3 times weak magnetic field, and the stability curve of the motor after 60min operation (ambient temperature 40 °C) calculated by using the transient temperature field are shown in Figs. 8-11.

As shown in Fig.8, the no-load induction back of EMF after the slots are skewed has a good sinusoidal degree. And the RMS of no-load phase voltage is 150.6 V.

As shown in Fig.9 to Fig. 11, the average output torque is 14.25 kN.m (power is 111.9 kW) at the rated speed of 75 r/ min, the output torque of the motor is 4.812 kN.m (power is 113.3 kW) at a constant power area of 225 r/ min, the RMS of motor current is 250 A(353.61/sqrt(2)), and the phase terminal voltage is 200.71 V((283.8/sqrt(2))) (line terminal voltage is 347.62 V), which meets the output voltage capacity of the frequency converter. It shows that the motor can achieve 3 times constant power flux weakening.

As shown in Fig.12, the highest temperature is 94 °C after the motor runs for 60 minutes, and the temperature rises about 54 K. The highest temperature appears at the end of the stator winding, and the rotor magnetic steel temperature is about 52 °C. Natural cooling is safe and reliable for

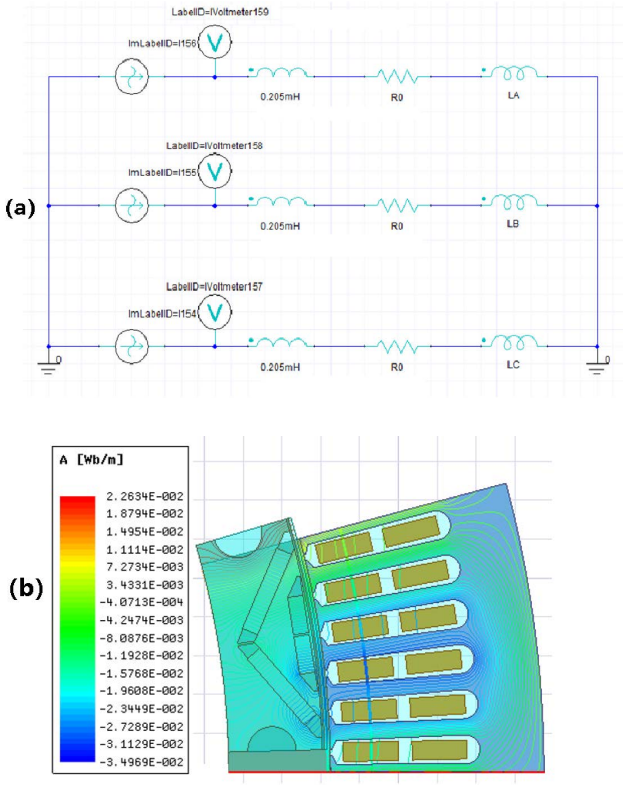

FIGURE 7. A simulation model based on field-circuit coupling analysis. a is stator circuit model of PMSM, and b is FEA model of the motor with interior V +− shape.

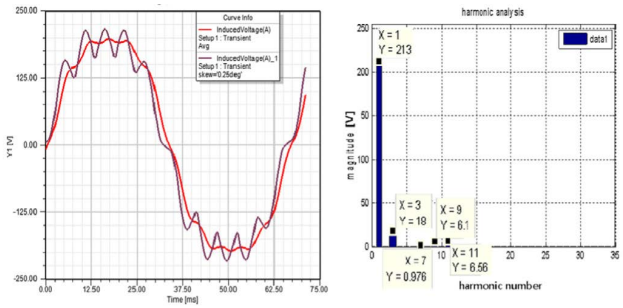

FIGURE 8. No-load induction back EMF FFT(skewed slots).

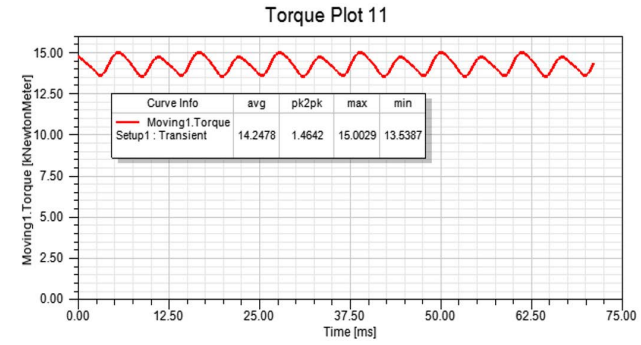

FIGURE 9. Torque curve at rated load.

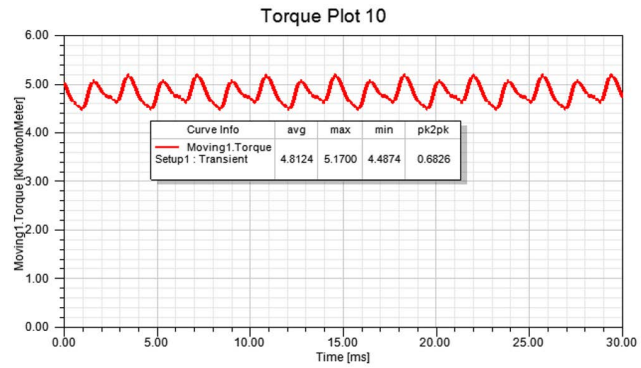

FIGURE 10. Torque curve at 3 times Flux-weakening level.

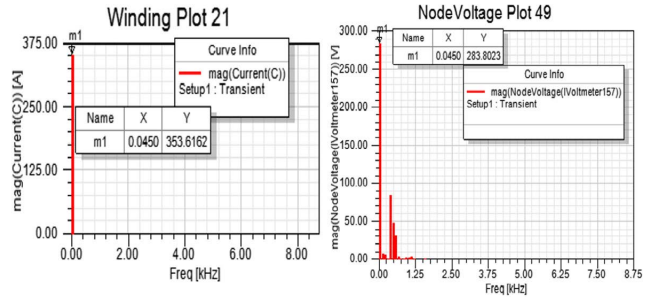

FIGURE 11. Current and terminal voltage FFT at 3 times Flux-weakening level.

short-time S2 (30 minutes) and 180 °C UH class permanent magnetic.

C. CO-SIMULATION ANALYSIS BASED ON CONSTANT TENSION

The linear velocity V_2 on the outside of the reel must also remain constant to maintain constant tension. Then, when V_2 remains constant, the speed of the motor decreases with the increase of the coil diameter, which is as follows

$$\mathrm{n} = \frac{V_2 i}{\pi D} \tag{19}$$

where V_2 is the linear velocity, i is the ratio of the drum, and D is the diameter of drum. the torque of drum can be given below.

$$\mathrm{T} = \mathrm{F}\frac{D}{2} \tag{20}$$

Therefore,the product of torque and speed is obtained as

$$T \cdot \mathrm{n} = F\frac{D}{2}\frac{V_2 \mathrm{i}}{\pi D} = F\frac{V_2 \mathrm{i}}{2\pi} = KF \tag{21}$$

here, $\mathrm{K} = \frac{V_2 i}{2\pi}$, when V_2 remains constant, K is constant, and F is constant tension.

The MotorSolve+Simulink co-simulation based on vector analysis is shown in Fig.13.Only part of the simulation curves of determining solutions is given because of the limitation of space. The co-simulation torque curve, current curve,

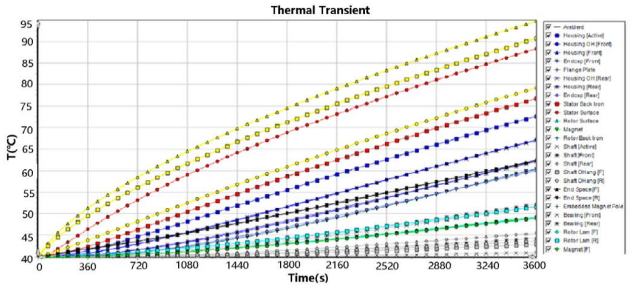

FIGURE 12. Motor temperature calculation curve.

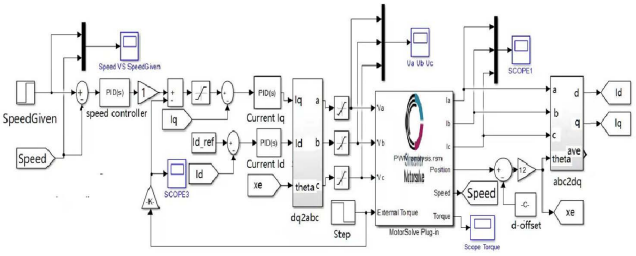

FIGURE 13. MotorSolve and Simulink simulation based on vector analysis.

and speed response curve under constant tension are shown in Fig. 13-15, respectively.

As shown in Figs.13-15, the major conclusions are listed as follows:

(1) The torque curve and the speed curve have a certain overshoot, and the speed regulation performance is good, and the load steady-state error is relatively small, 14000 N.m load about 0.02 seconds to restore the given speed. Under constant tension control, the speed response under the given speed curve has good tracking performance. Error and overshoot are small.

(2) The method of MotorSolve and Simulink co-simulation can optimize motor parameters from the perspective of system matching, which is more in line with reality.

V. DEMONSTRATION APPLICATION AND TEST

A low-speed and high-efficiency PMSM and a driving frequency converter were manufactured to verify the analysis results and the correctness of the method. The demonstration application and test were carried out on a 45 T EWMW in a deep-sea test platform, as shown in Fig.16.Then, it was certified by the China Classification Society.The pre-interference and post-processing waveforms of rotating transformer signals are shown in Fig.17, respectively. It is obvious that the transition plate of non-magnetic material reduces the interference of the brake to the position signal, and the effect is obvious. The measured line voltage curve of the motor under rated load is shown in Fig.18, and the aver RMS of line voltage is 288.5 V. TABLE 3 shows that the part of the simulation agrees well with those measured values.

The main conclusions by the simulation analysis and test are listed as follows:

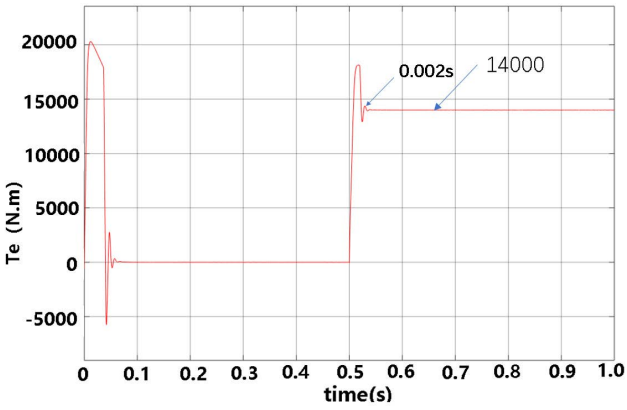

FIGURE 14. Torque curve of the PMSM.

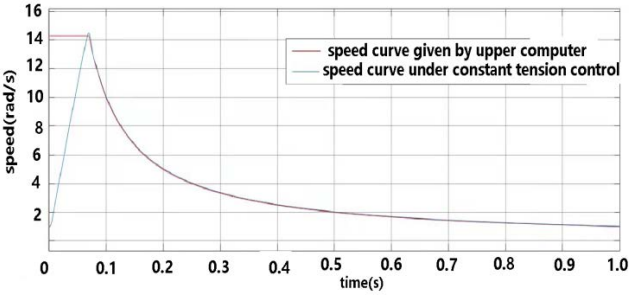

FIGURE 15. Speed response curve under constant tension.

FIGURE 16. Demonstration application and testing of prototype.

FIGURE 17. Waveforms before and after the interference of the rotary transformer signal.

(1) The PMSM simulation value is in good agreement with the actual test value. The motor can meet three times the field weakening speed regulation and 2.3 times the short-time

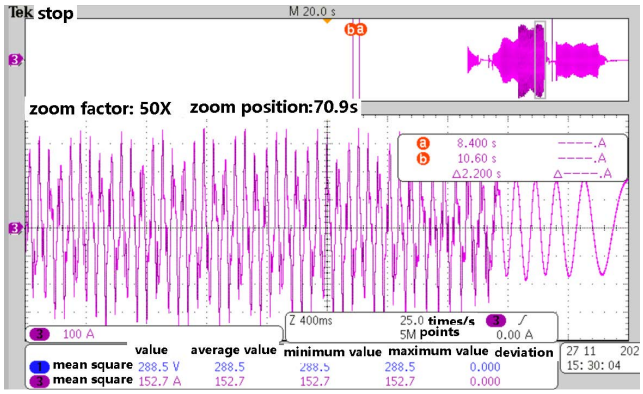

FIGURE 18. Line-voltage curve.

TABLE 3. Simulation and test data.

ITEM	The results of FEA	The results of test
Rated line voltage / V	285	288.5
Rated line current / A	250	248.6
Rated torque / kN.m	14.25	14.33
Line terminal voltage (under 225r/min) /V	347.62	352.5
Time of 2.3 times overload torque	2s	3s
Efficiency of motor /%	93.5	94.3
Temperature rises /k (60min)	54	45.5

overload capacity. The measured value of motor efficiency is 94.3%, The gear efficiency is about 96%, the inverter efficiency is 98.3%, and the motor efficiency is 94.3%. Therefore, the efficiency of the system can be easily obtained as $0.96 \times 0.983 \times 0.943 = 88.9\%$.

The error between the calculated temperature rise (50 K) and the PMSM experimental value (45.5 K) is about 8.5 K. The main reason is that the actual motor base and casing are connected to the WMW and have good thermal conductivity. Therefore, the actual short-time operation of the motor for 30 minutes adopts natural cooling, which fully meets the requirements, and the operation is safe and reliable.

(2) The accuracy of the position signal of PMSM has a great influence on the constant tension control of the EWMW and the follow-up and dynamic response of the large impact load. In this paper, it is proposed that after the magnetic isolation measures of non-conductive materials and the large gap of the reluctance resolver are adopted, the electromagnetic field of the electromagnetic brake has little interference to the signal of the position sensor, and the waveform is perfect.

(3) The permanent magnetization drive system of EWMW is a complex and large-scale system, involving the motor and its drive, upper computer communication, control, mechanical transmission, etc., which needs to be further studied.

VI. CONCLUSION

The design and application of low-speed and high-efficiency PMSM and drive systems are difficult due to the special load characteristics and requirements of EWMW. Taking a set of 110kW 75r / min PMSM and its drive system as an example, a parameter matching design method of low-speed and high-efficiency PMSM based on finite element, field circuit coupling, and co-simulation is proposed in this paper. At the same time, it also describes some design matters of structural matching. Finally, through the development of the prototype and the demonstration application and test on the 45t electric anchor winch, the test results show that the performance indexes fully meet the design requirements and verify the correctness and effectiveness of the matching design method. It has certain reference and guiding significance for the design and application of PMSM and drive system of WMW.

REFERENCES

[1] D. Lee and S. Chun, "Characteristics of ship winches and their hydrostatic drives," *J. Korea Soc. Fluid Power*, vol. 4, no. 2, pp. 27–34,2007.

[2] S. Ji, S. Kim, and Y. Kim, "Experimental approach for mooring winch control system design," in *Proc. ICCAS*, Gwangju, South Korea, 2013, pp. 1025–1028.

[3] Q. Chen, W. Li, and G. Chen, "FUZZY P+ID controller for a constant tension winch in a cable laying system," *IEEE Trans. Ind. Electron.*, vol. 64, no. 4, pp. 2924–2932, Apr. 2017.

[4] Z. Shuzhong, "Development of automation control technology for anchor winch," *J. Mar. Electr. Technol.*, vol. 32, no. 4, pp. 46–49, Apr. 2012.

[5] K. Atallah, D. Howe, P. H. Mellor, and D. A. Stone, "Rotor loss in permanent-magnet brushless AC machines," *IEEE Trans. Ind. Appl.*, vol. 36, no. 6, pp. 1612–1618, Nov./Dec. 2000.

[6] M. R. Shah, J. P. Alexander, S. Galioto, K.-K. Huh, and W. D. Gerstler, "Rotor end losses in multi-phase fractional-slot concentrated-winding permanent magnet synchronous machines," in *Proc. IEEE Energy Convers. Congr. Expo.*, Sep. 2010, pp. 1312–1320.

[7] J. Cros and P. Viarouge, "Synthesis of high performance PM motors with concentrated windings," *IEEE Trans. Energy Convers.*, vol. 17, no. 2, pp. 248–253, Jun. 2002.

[8] N. Bianchi, L. Alberti, and O. Bottesi, "Energy efficiency improvement adopting synchronous motors," *Int. J. Comput. Math. Electr. Electron. Eng.*, vol. 34, no. 1, pp. 76–91, Jan. 2015.

[9] K.-C. Kim, J. Lee, H. J. Kim, and D. H. Koo, "Multiobjective optimal design for interior permanent magnet synchronous motor," *IEEE Trans. Magn.*, vol. 45, no. 3, pp. 1780–1783, Mar. 2009.

[10] P. H. Damen and F. Gardner, "Linear PM Generator system for wave energy conversion in the AWS," *IEEE Trans. Energy Convers.*, vol. 19, no. 3, pp. 583–589, Sep. 2006.

[11] M.-R. Park, H.-J. Kim, Y.-Y. Choi, J.-P. Hong, and J.-J. Lee, "Characteristics of IPMSM according to rotor design considering nonlinearity of permanent magnet," *IEEE Trans. Magn.*, vol. 52, no. 3, pp. 1–4, Mar. 2016.

[12] X. Liu, H. Chen, J. Zhao, and A. Belahcen, "Research on the performances and parameters of interior PMSM used for electric vehicles," *IEEE Trans. Ind. Electron.*, vol. 63, no. 6, pp. 3533–3545, Jun. 2016.

[13] K.-T. Kim, K.-S. Kim, S.-M. Hwang, T.-J. Kim, and Y.-H. Jung, "Comparison of magnetic forces for IPM and SPM motor with rotor eccentricity," *IEEE Trans. Magn.*, vol. 37, no. 5, pp. 3448–3451, Sep. 2001.

[14] D. Howe and Z. Q. Zhu, "The influence of finite element discretization on the prediction of cogging torque in permanent magnet excited motors," *IEEE Trans. Magn.*, vol. 28, no. 2, pp. 1080–1083, Mar. 1992.

[15] D. Joo, J.-H. Cho, K. Woo, B.-T. Kim, and D.-K. Kim, "Electromagnetic field and thermal linked analysis of interior permanent-magnet synchronous motor for agricultural electric vehicle," *IEEE Trans. Magn.*, vol. 47, no. 10, pp. 4242–4245, Oct. 2011.

[16] J. Chen, C. V. Nayar, and L. Xu, "Design and finite-element analysis of an outer-rotor permanent-magnet generator for directly coupled wind turbines," *IEEE Trans. Magn.*, vol. 36, no. 5, pp. 3802–3809, Sep. 2000.

[17] G. Zhou, X. Xu, Y. Xiong, and L. Zhang, "Design and analysis of low-speed high torque direct-driven permanent magnet synchronous machines(PMSM) with fractional-slot concentrated winding used in coal mine belt conveyor system," in *Proc. 20th Int. Conf. Electr. Mach. Syst. (ICEMS)*, Aug. 2017, pp. 1–5.

[18] J. Zhang, B. Zhang, G. Feng, and B. Gan, "Design and analysis of a low-speed and high-torque dual-stator permanent magnet motor with inner enhanced torque," *IEEE Access*, vol. 8, pp. 182984–182995, 2020.
[19] N. Bianchi, S. Bolognani, and P. Frare, "Design criteria for high-efficiency SPM synchronous motors," *IEEE Trans. Energy Convers.*, vol. 21, no. 2, pp. 396–404, Jun. 2006.
[20] S. Morimoto, M. Sanada, and Y. Takeda, "Variable speed drive system of interior permanent magnet synchronous motors for constant power operation," in *Proc. PCC-Yokohama*, 1993, pp. 402–407.
[21] M. Sanada, S. Morimoto, and Y. Takeda, "Design of permanent magnet linear synchronous motors for wide speed operation and end effect," presented at the Nat. Conv. Inst. Electr. Eng. Jpn., 1995.
[22] T. M. Jahns, "Flux-weakening region operation of an interior permanent magnet synchronous motor drive," *IEEE Trans. Ind. Appl.*, vol. IA-23, no. 4, pp. 681–689, Aug. 1987.
[23] F. Gui-Hong, L. Qing-Xu, Z. Bing-Yi L. Zhong-Qi, and L. Hao, "Speed adjusting ability with field weakening of permanent magnet motor for electric vehicle," *Electric Mach. Control*, vol. 18, pp. 55–66, Oct. 2014.
[24] C. Renyuan, "A new structure of permanent magnet traction motor for improving flux-weakening level," *Trans. China Electrotechnical Soc.*, vol. 27, pp. 100–104, Oct. 2012.
[25] S. L. Ho, H. L. Li, W. N. Fu, and H. C. Wong, "A novel approach to circuit-field-torque coupled time stepping finite element modeling of electric machines," *IEEE Trans. Magn.*, vol. 36, no. 4, pp. 1886–1889, Jul. 2000.
[26] J. Chao, Q. Mingzhong, P. Wei, and Z. Zhibin, "Design and analysis of high-power density permanent magnet synchronous motor for warship pump," *Micromotors*, vol. 52, pp. 1–6, Nov. 2019.
[27] T. Rudnicki, A. Sikora, R. Czerwinski, and T. Glinka, "Impact of PWM control frequency on efficiency of drive with 1 kW permanent magnet synchronous motor," *Int. J. Comput. Math. Electr. Electron. Eng.*, vol. 37, no. 1, pp. 307–318, Jan. 2018, doi: 10.1108/COMPEL-01-2017-0031.

GUI-HOU ZHOU received the B.S. degree in electronic engineering from Wuhan University, in 2002, and the M.S. degree in electrical machines from the Wuhan Institute of Marine Electric Propulsion, Wuhan, China, in 2008. He is currently pursuing the Ph.D. degree with the College of Electrical Engineering, Naval University of Engineering.

In 2008, he joined the Wuhan Institute of Marine Electric Propulsion, and worked on the design and analysis of special electric machines, especially the high-efficiency low vibration and noise motor permanent magnet synchronous motor. His research interests include vibration and noise control of PMSM, electromagnetic field analysis, structural design of electric propulsion motor, and marine auxiliary machinery.

MING-ZHONG QIAO received the B.S. and Ph.D. degrees in electrical engineering from the Naval University of Engineering, Wuhan, China, in 1996 and 2003, respectively. He is currently a Professor with the Department of Electrical Engineering, Naval University of Engineering. His current research interests include power system automation and ship propulsion motor.

XIAO-FENG ZHANG received the B.S. and M.S. degrees in electrical engineering from the College of Electrical Engineering, Naval University of Engineering, Wuhan, China, in 1982 and 1985, respectively, and the Ph.D. degree from Tsinghua University, Beijing, China, in 1996. Since 1997, he has been a Professor with the College of Electrical Engineering, Navy University of Engineering. His major research interest includes power system automation of shipboard.

JIN-HUI XIE received the B.S. degree in control engineering from Tianjin University, China, in 1984.

In 1984, he joined the Wuhan Institute of Marine Electric Propulsion, Wuhan, China. His research interests include ship power stations and electric propulsion equipment.

QING-LIANG HAO received the B.S. degree in electrical machines from the Taiyuan University of Technology, China, in 2001, and the M.S. degree in electrical machines from the Huazhong University of Science and Technology, China, in 2011. In 2001, he joined the Wuhan Institute of Marine Electric Propulsion, Wuhan, China. His research interests include vibration and noise control of PMSM and ship power stations and electric propulsion equipment.

CONG WAN received the M.S. degree in control engineering from the Wuhan University of Technology, China, in 2012. In 2012, he joined the Wuhan Institute of Marine Electric Propulsion, Wuhan, China. His research interests include power electronics and its control.

YONG ZHOU received the B.S. and M.S. degrees in marine engineering from the Wuhan University of Technology, China, in 2004 and 2007, respectively. He is currently pursuing the Ph.D. degree with the College of Civil Engineering and Mechanics, Lanzhou University. In 2007, he joined the Wuhan Institute of Marine Electric Propulsion, Wuhan, China, and worked on the design and analysis of special electric machines, especially the high-temperature super-conducting motor and high-speed permanent magnet synchronous motor with high power density. His research interests include vibration and noise control, composite material design, and structural design of electric machines.